Int J Adv Manuf Technol (2018) 95:257–266
https://doi.org/10.1007/s00170-017-1190-4

ORIGINAL ARTICLE

The effects of the silicon wafer resistivity on the performance of microelectrical discharge machining

Noor Dzulaikha Daud[1] · **Alaa AbuZaiter**[2] · **Pei Ling Leow**[1] · **Mohamed Sultan Mohamed Ali**[1]

Received: 16 June 2017 / Accepted: 3 October 2017 / Published online: 18 October 2017

Abstract In this study, the performance of Si wafer machining by employing the die-sinking microelectrical discharge machining technique is reported. Specifically, the machining performance was examined on both high- (1–10 Ω cm) and low-resistivity (0.001–0.005 Ω cm) Si wafers by means of using a range of discharge energies. In this regard, the machining time, material removal rate, surface quality, surface roughness, and material mapping, which are categorized among the important properties in micromachining, have been investigated. In order to analyze the surface properties and to perform the elemental analysis, the scanning electron microscope and energy-dispersive X-ray spectroscopy were used. In contrast, the 3D surface profiler was used to evaluate the roughness of machined surface. The results of this experimental study revealed that the electrical resistivity and discharge energy parameter of microelectrical discharge machining had a great influence on the Si wafer machining performances. The observations in this study indicated a decrease in machining time, high material removal rate, and high surface roughness with an increased discharge energy values. Overall, it was learnt that the minimum amount of energy required to machine Si wafer was 5 μJ for both low and high-resistivity Si. In addition, the highest material removal of 5.842×10^{-5} mm^3/s was observed for low-resistivity Si. On the contrary, the best surface roughness, R_a, of 0.6203 μm was achieved for high-resistivity Si and it also pointed to a higher carbon percentage after the machining process.

Keywords Microelectrical discharge machining · Si machining · Machining performance · Material removal rate

1 Introduction

Owing to its superior mechanical and electrical properties which can be precisely controlled, Si has therefore become a fundamental substrate in semiconductor and electronics industry [1]. In addition, the Si has been described in various studies as a hard to machine material because of its high brittleness and low fracture toughness [2], which resulted in its poor machinability [3]. It can also be seen in the literature that the conventional machining techniques such as the chemical etching help provide solutions for two-dimensional (2D) machining of Si wafers. On the contrary, the 3D machining techniques are not considered as feasible due to the crystal orientations of Si and line-of-sight etching [4]. Besides, some scholars have argued that the material removal rate (MRR) of the chemical etching process is rather slow, and therefore, the desired shape of etching may not be able to be controlled as a result of the anisotropic and isotropic nature of such a process. Notably, the desired specifications of aspect ratio and 3D microfeatures are required by most of the microelectromechanical system (MEMS) applications such as the optical devices, sensors, and actuators. It is worthy of note that such requirements culminated in the introduction of various novel machining methods such as laser beam [5], ultrasonic [6] and focused ion beam (FIB) milling [7] with the aim of producing high-quality 3D freeform shapes of Si. Related studies have proven that such unconventional machining techniques are capable of producing 3D features.

✉ Mohamed Sultan Mohamed Ali
sultan_ali@fke.utm.my

[1] Faculty of Electrical Engineering, Universiti Teknologi Malaysia, 81310 Skudai, Johor, Malaysia

[2] Department of Engineering, Palestine Technical College, Deir El Balah, Gaza, Palestine

Notwithstanding such potentials, there are certain setbacks such as the thermal damage [8], crack formation [9], and low MRR [10]. Along with such issues, the high installation cost is also seen as equally a limiting factor. It is worth highlighting that the μEDM is one of the unconventional techniques that offers noncontact machining in order to help reduce the tendency of crack propagation on the Si wafer as it is usually the case in the laser beam and ultrasonic machining techniques [11]. Also interestingly, it is capable of machining any conductive materials including pure metals such as Cu [12] and metal matrix composite material (MMCs) like Inconel 825 alloy [13], Aluminum 6351 alloy [14] and Nitinol [15–17] without having to depend on its mechanical properties such as the strength, toughness, and brittleness [2]. In relation to its applications, μEDM has widely been utilized to pattern the carbon nanotube forest [18, 19] and conductive polymers [20]. As some related studies have proven, this method is known to remove the material by erosive action of electrical discharge between an electrode and a workpiece, which is separated by dielectric fluid [21]. μEDM involves relatively lower capital equipment cost [22] and it has multiple axes of movements, which makes it more suitable for the machine complex 3D shapes [23]. Attempts to control the machining rate of μEDM can be carried out by altering the settings of the discharge generator. It has to be noted that such a function further promotes the μEDM as an ideal material removal method in machining Si wafers irrespective of their hardness. In the literature, it was found that several studies have identified new methods in order to increase machinability, efficiency, and performance of Si machining by means of using μEDM technique. More importantly, the electrical conductivity of the Si wafer is considered as the main parameter in relation to the machinability by means of using μEDM. In the event of the surface potential barriers that appear to prevent the discharge current, plating or coating the Si wafer with a conductive layer such as gold [24], gold-antimony [25], and Cu [26] to provide electrical conductivity has been widely carried out, as discussed in related studies. On the other hand, the characterization performances in relation to the efficiency, speed, and surface roughness have been widely looked into for wire electrical discharge machining (WEDM) technique of Si material [27–29]. In addition, some other studies have also explored the machining rate, stability, and EDM-induced surface [29, 30]. It has been proven in a number of research that the electrical resistivity, which is actually the response to the electrical conductivity, may also have a great impact on the performance of μEDM. To the best knowledge of the researchers, studies that have reported on the effects of the Si material's resistivity on μEDM machining performances are really scarce.

The present study reports the findings upon looking into the Si wafers machining performance of die-sinking μEDM technique in relation to the MRR, surface quality, surface roughness, and material mapping. In order to make the characterization more comprehensive, the machining performance was evaluated on two different Si wafers with different resistivity by means of using a range of discharge energies (DE) to help evaluate the effects of the material's resistivity on the machining performances. In this regard, the quality of the machined cavities was looked into experimentally through surface profiling, scanning electron microscope analysis (SEM), and energy-dispersive X-ray spectroscopy (EDX) to help provide a better understanding on the quality of machining.

2 Experimental setup

The machine that was used in this die-sinking μEDM experiment is Hybrid μEDM (DT-110, Mikrotools, Singapore) that offers three axes of movement: x, y, and z, which can be controlled by means of using numerical control (NC) codes. The schematic diagram of the die-sinking μEDM setup can be seen in Fig. 1a. The polarity for the tool electrode and the Si wafer was set to be negative (i.e., cathode) and positive (i.e., anode), respectively. Both the tool electrode and workpiece were immersed in a tank, which was filled with dielectric oil (DIEL MS 5000) as shown in Fig. 1b. In addition, the basic properties of the dielectric oil are presented in the Table 1. A 3-mm-diameter brass rod (58% Cu, 39% Zn, and 3% Pb) had to be selected as the material for electrode towing to its relatively higher electrical conductivity. By means of engaging in the microturning process with a diamond cutter, the electrode diameter was able to be narrowed down to 300 μm. As for the workpiece material, n-type (i.e., phosphorus dopant) Si wafers with the size of 1 cm × 1 cm were used. In order to investigate the effects of Si resistivity on machining performance, two single-sided polished n-type Si wafers with differences in resistivity were prepared for the experiment. The first sample is the low-resistivity Si ([1 0 0] n-type, resistivity of 0.001–0.005 Ω cm and thickness of 500 μm), in contrast to the second sample that has higher resistivity ([1 0 0] n-type, resistivity of 1–10 Ω cm and thickness of 500 μm).

The DEs were defined by tuning the voltage and discharge capacitor of the machine controller circuit. By disregarding stray capacitances found in the circuit and at the same time, assuming the full voltage of the discharge capacitor, the DE can therefore be expressed by the following Eq. 1:

$$DE = \frac{CV^2}{2} \tag{1}$$

where C represents the capacitance and V as the open-circuit voltage [31]. Two variables were taken into account in the course of the experiments: voltage which was set from 80 to 120 V in interval of 10 V, and capacitance was set in the range

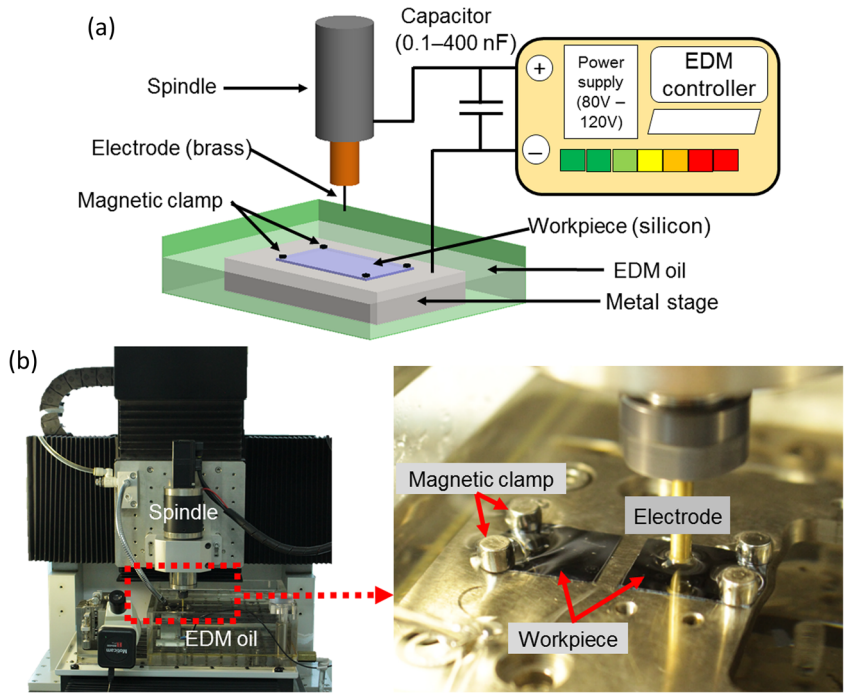

Fig. 1 Die-sinking μEDM experimental setup (**a**) schematic diagram (**b**) actual setup during machining of Si sample

of 0.1 to 400 nF in order to obtain various parameters of DE. As a result, the variable DE is produced within the range of 0.5 to 2000 μJ. In this regard, the machining parameters used in the die-sinking μEDM are summarized in Table 2.

The experiment began by means of fixing both samples on the machine fixture inside the tank through the utilization of the magnetic clamps. In order to immerse the sample, the tank had to be filled with dielectric EDM oil. In the course of the machining process, the rotation speed of the electrode was set at 3000 rpm. In addition, the gap identified between the sample and electrode was controlled within 3–5 μm. The cavities with 100 μm depth were machined with a feed rate of 50 μm/min in *z*-axis. In order to characterize the performance, the strategy of machining was selected to drill nine cavities in low-resistivity sample using different values for the voltage and capacitance (as summarized in Table 2) starting with 80 V and 10 nF. These values were varied to achieve nine DE, as indicated in Table 2. It is worthy of note that the tool electrode is flatted using the diamond cutter before each cavity formation. Similar steps are repeated for high-resistivity sample and the results are compared in Section 3.

Table 1 Properties of dielectric oil (DIEL MS 5000)

Basic physical and chemical properties	Remarks
Dielectric constant, ε_r	1.795
Density at 15 °C	816 kg/m^3
Flash point	> = 120 °C
Kinematic viscosity	3.9 mm^2/s at temperature 40 °C
	6.5 mm^2/s at temperature 20 °C

The machining time was recorded based on the coordinate movement through *z*-axis with time. In the case of the present study, the MRR was calculated by means of using the following Eq. 2:

$$\mathrm{MRR} = \frac{\pi \times r^2 \times L \ (\mathrm{mm}^3)}{\text{machining time (sec)}} \tag{2}$$

where r is the radius of cavity and L is cavity depth that can be achieved for each machined cavity. In this regard, the MRR value was calculated based on the ratio of the volume of the material removed to the machining time.

Table 2 Experimental conditions

Parameters	Values used
Open-circuit voltage (V)	80, 90, 100, 110, 120
Capacitor (nF)	0.1, 1, 10, 100, 400
Discharge energy (μJ)	0.5, 5, 30, 40, 50, 60, 70, 500, 2000
Electrode material	Brass
Electrode diameter (μm)	300
Electrode rotation speed (rpm)	3000
Feed rate during EDM (μm/min)	50
Depth of cavity (μm)	100
Polarity	Tool negative
Machining environment	Dielectric oil, DIEL MS 5000

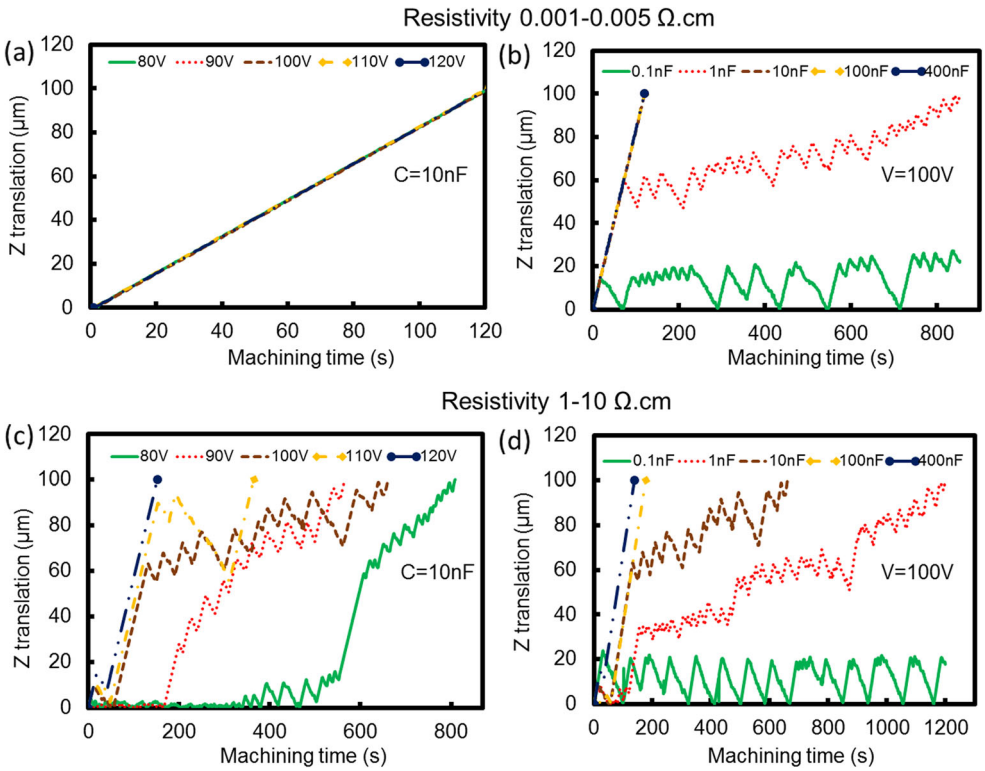

Fig. 2 Machining time for 100 μm depth: low-resistivity sample **a** voltage varied, **b** capacitance varied: high-resistivity sample, **c** voltage varied, and **d** capacitance varied

3 Results and discussion

3.1 Machining time

Based on the die-sinking μEDM experimental setup and settings conditions shown in Fig. 1 and Table 2, the total machining time for each parameter is recorded and plotted in Fig. 2. The results indicated that the increase in voltage and capacitance decreases the time required to machine cavity of 100 μm depths. The high voltage and capacitance produced high DE to remove the workpiece material at high speed, and as a result, machining time became shorter. In order to avoid short circuit, which leads to unstable machining process, spark gap, i.e., the gap between electrode and workpiece, was controlled to be 3–5 μm [32]. However, when short circuit was detected, the tool electrode-workpiece gap was increased by 5 μm by means of retracting the *z*-axis before approaching the workpiece again with pre-set feed rate which is maintained at 50 μm/min during the normal machining process. The results in Fig. 2 showed that the machining time with voltage variation from 80 to 120 V with 10 nF capacitor for low-resistivity sample (see Fig. 2a) and high-resistivity sample (see Fig. 2c) can be completed within 810 s. As regards, the capacitance variation from 0.1 to 400 nF with 100 V for low-resistivity

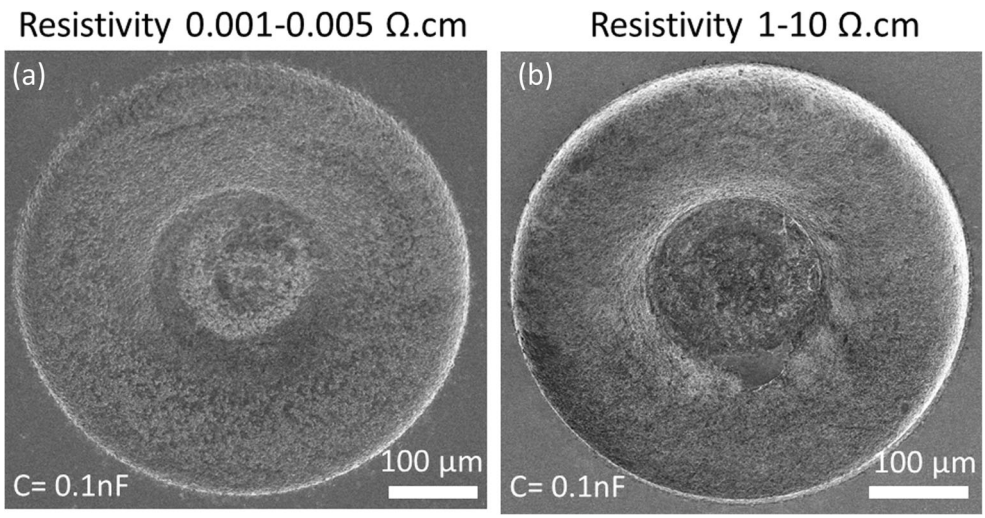

Fig. 3 SEM images of cavity machined using 100 V with 0.1 nF for both samples

sample (see Fig. 2b) and high-resistivity sample (see Fig. 2d), it was observed that 100 μm cavity can be machined for all the parameters except for the lowest capacitance, 0.1 nF with 100 V, which stopped at 27 μm for low-resistivity sample within 854 s and 23.9 μm for high-resistivity sample within 1200 s. This observation is explained based on Eq. 1, where the value of DE for the lowest capacitance, 0.1 nF with 100 V (0.5 μJ), was not high enough to drill a 100-μm cavity. In addition, both samples exhibited that the cavities are not fully machined, and as shown in Fig. 3, big craters are produced in the middle, which justify that 0.5 μJ cannot be selected as machine parameter. Hence, the researchers concluded that due to the sensitive short-circuit detection, the minimum DE required to machine the cavity is 5 μJ with a very long machining time.

In Fig. 2c, parameter of 80 and 90 V with 10 nF showed sharp increase pattern on the *z*-translation starting at 553 s (80 V, 10 nF) and 167 s (90 V, 10 nF). This condition happens due to low DE utilized to machine the cavity, which is 30 and 40 μJ that require long time to stabilize the machinability. The beginning of the machining process showed long short-circuit detection because of the difficulty to remove the workpiece material using low DE. With regard to high DE, 100 to 120 V, the *z*-translation pattern increased sharply during the earlier stage of the machining process because of high DE used to machine the cavity. The effect of different parameters on the cavity drilled by die-sinking μEDM to the machining time (see Fig. 2) indicated that low-resistivity sample has shorter machining time than high-resistivity sample. The machining

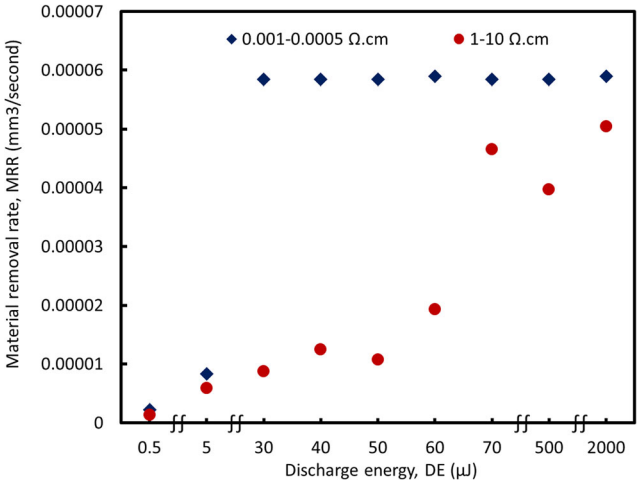

Fig. 4 Relationship between material removal rate of die-sinking μEDM process and increment DE for both samples

time is dependent on the resistivity value of the workpiece. The decrease in resistivity of the workpiece material will increase the ease of the μEDM machining. This is due to the fact that the electrical resistivity of the workpiece requires the transfer of electric current to create the discharge pulse.

3.2 Material removal rate

MRR is one of the important factors to study the efficiency of μEDM. In order to understand the efficiency of μEDM machining, the value of MRR has to be calculated based on Eq. 2.

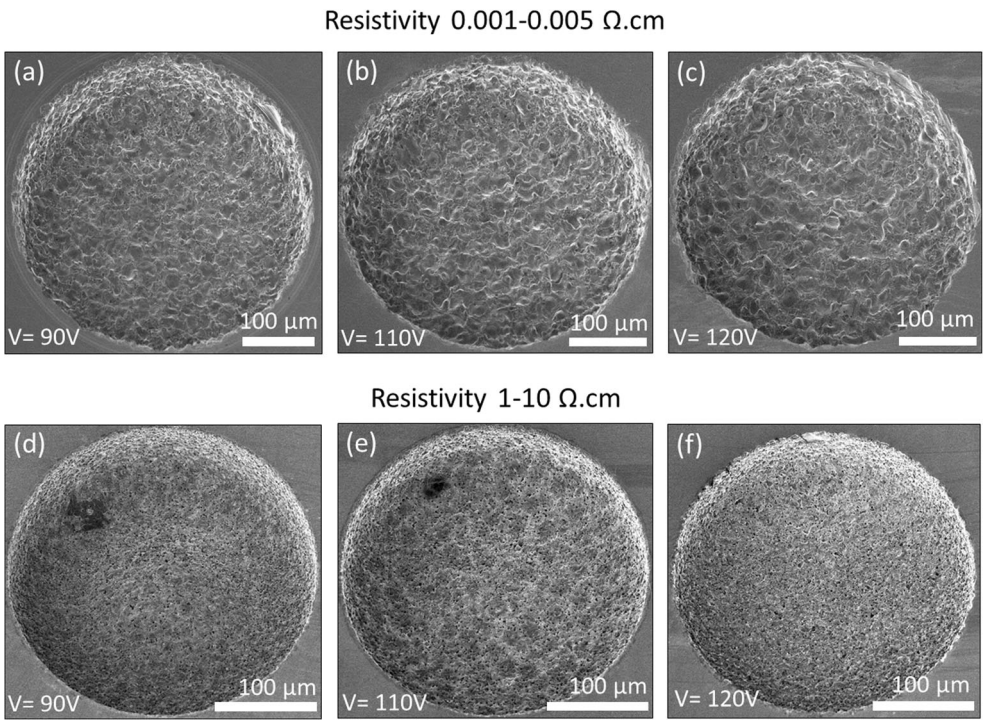

Fig. 5 SEM images of cavity machined by μEDM process with 10 nF and voltage value varied for: low-resistivity sample **a** 90 V, **b** 110 V, and **c** 120 V; high-resistivity sample **d** 90 V, **e** 110 V, and **f** 120 V

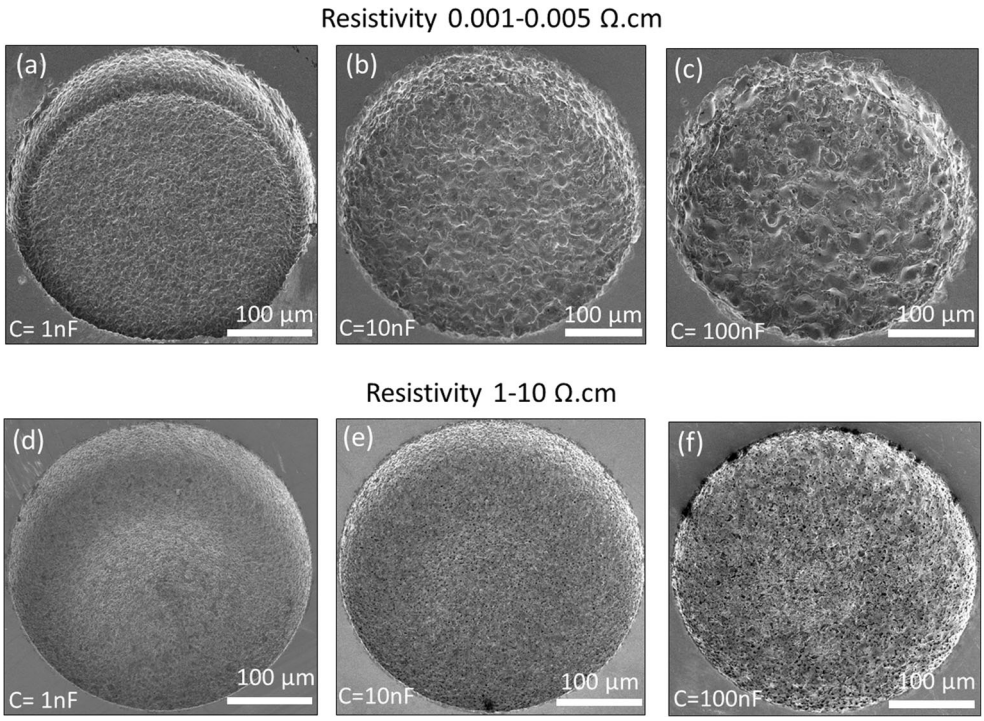

Fig. 6 SEM images of cavity machined by µEDM process with 100 V and capacitance value varied for: low-resistivity sample **a** 1 nF, **b** 10 nF, and **c** 100 nF; high-resistivity sample **d** 1 nF, **e** 10 nF, and **f** 100 nF

Figure 4 presents the MRR for both low- and high-resistivity samples. The graph indicated that the MRR values increased with the increasing value of DE. Nevertheless, when low value of DE was employed, it resulted in low MRR value due to the occurrence of short-circuit detection, which caused instability in machining process. Figure 4 demonstrated that low-resistivity sample has relatively higher MRR than high-resistivity sample. Consequently, the low-resistivity sample exhibited machining that is stable as discussed in Section 3.1. MRR for low-resistivity sample reached the maximum value of 5.842×10^{-5} mm^3/s when DE reached 30 µJ. If the feed rate value is increased, these values of MRR can be improved further. As regards the high-resistivity sample, the nonlinear graph pattern is observed. The high-resistivity sample started to be machined at 5 µJ and reached the maximum MRR at 2000 µJ. However, beyond 70 µJ, the increase in MRR value did not improve much and instable MRR trend is observed. This is most likely due to the differences in machining parameter being used for difference DE as disclosed in Table 2. Overall, the resistivity of the materials has great influence on MRR.

3.3 Surface quality

The surface analysis of machined cavities was performed qualitatively by means of a field emission scanning electron microscope (FESEM) with an energy-dispersive X-ray spectroscopy (SU8020, Hitachi, Japan). Figures 5 and 6 present the images of the results of machined cavity using various parameters to study the quality of the machining with different resistivities and values of DE. The effects of voltage and capacitance parameters on both low- and high-resistivity

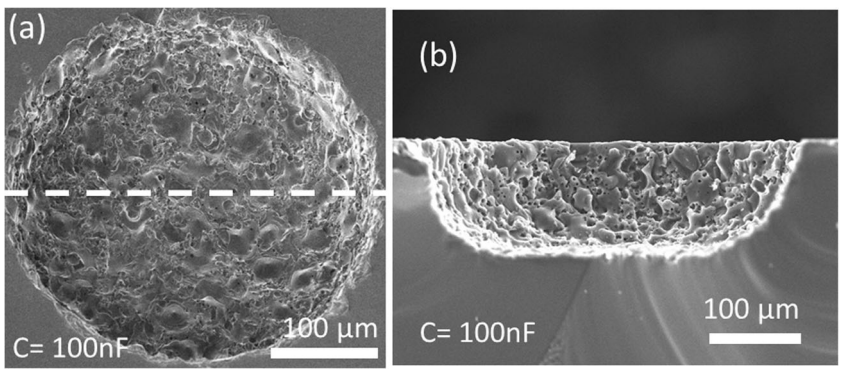

Fig. 7 Low-resistivity sample cavity machined by µEDM process with high capacitance of 100 nF with 100 V **a** top view and **b** cross-sectional view

samples are shown in Figs. 5 and 6. Figure 5a–c and Fig. 6a–c exhibited low-resistivity sample, and large size of crater is generated. Moreover, Fig. 5d–f and Fig. 6d–f showed high-resistivity sample, and small size features are created. It has to be noted that in Fig. 5a, d, low voltage value of 90 V with 10 nF was utilized. In Fig. 6a, d, low capacitances value of 1 nF with 100 V was used and it was discovered that smaller craters were created on the machined surface of high-resistivity sample compared to low-resistivity sample. This might be due to the low capacitance of 1 nF of the DE value used, which was inadequate and ineffective to remove material with higher resistivity. With regard to the high-voltage parameters of 110 and 120 V with 10 nF (see Fig. 5b, c, e, and f) and high-capacitance parameters of 10 and 100 nF with 100 V (see Fig. 6b, c, e, and f), large size and high amount of craters were formed. For low-resistivity sample, the cross-sectional view of the cavity machined with 500 μJ is shown in Fig. 7b along the line presented in Fig. 7a. The increase in voltage and capacitance values produced a strong DE to remove the workpiece material at high speed, and subsequently, large craters have been generated on the surface.

3.4 Surface roughness

Surface roughness is the value of different cutting modes, which was quantitatively investigated by using a 3D surface profiler (S neox, Sensofar Metrology, Spain). This measurement is a combination of three techniques, namely, confocal, interferometry, and focus variation to calculate the values of surface roughness. The confocal technique was used to measure surface height from smooth to very rough surfaces as low as 0.1 μm. Interferometry technique was employed to measure surface height from smooth to moderately rough (providing nm) and very smooth (providing sub nm). The last technique, i.e., focus variation, was used to measure shape of large rough surfaces. Each cavity from both samples was analyzed based on the surface roughness value that was plotted against the DE as shown in Fig. 8, which indicated that the surface roughness increased with the increment of DE [33]. The low-resistivity

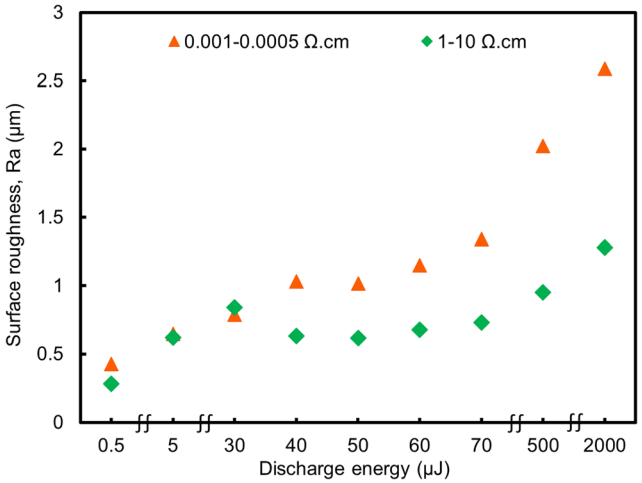

Fig. 8 Relationship between surface roughness of die-sinking μEDM process and increment of discharge energy for both samples

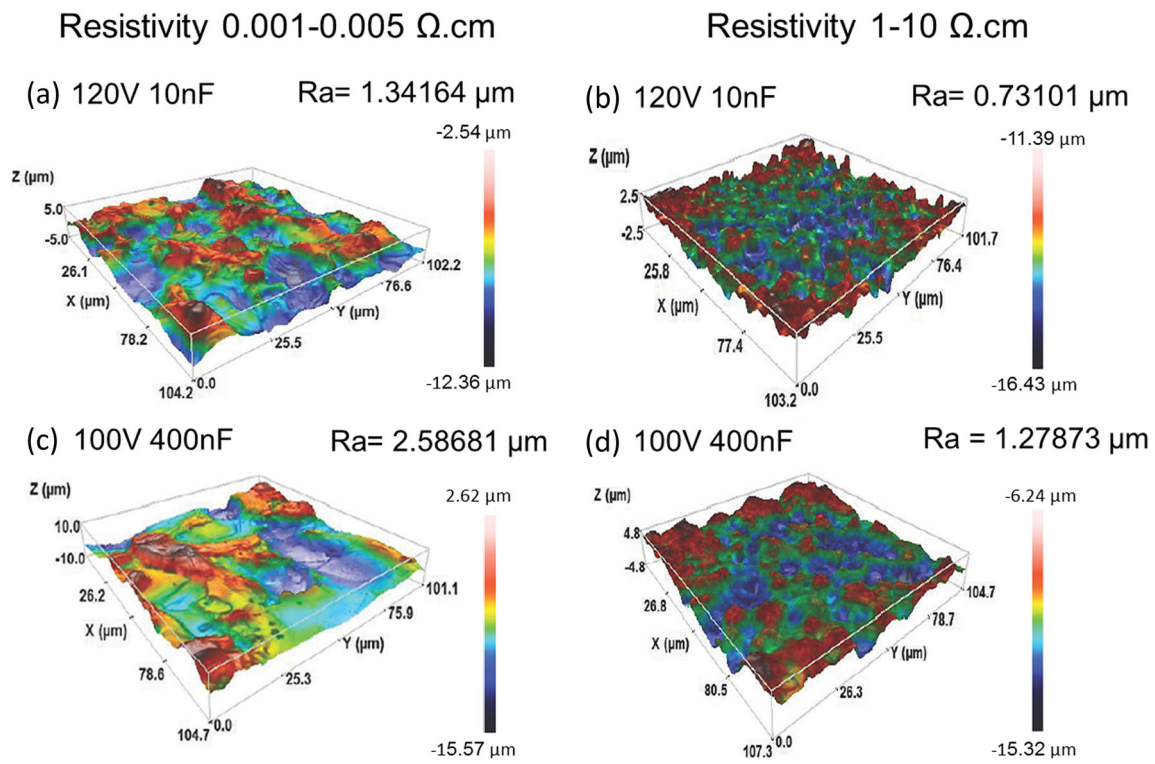

Fig. 9 Surface roughness for low-resistivity sample **a**120 V, **c** 400 nF; high-resistivity sample **b** 120 V, **d** 400 nF

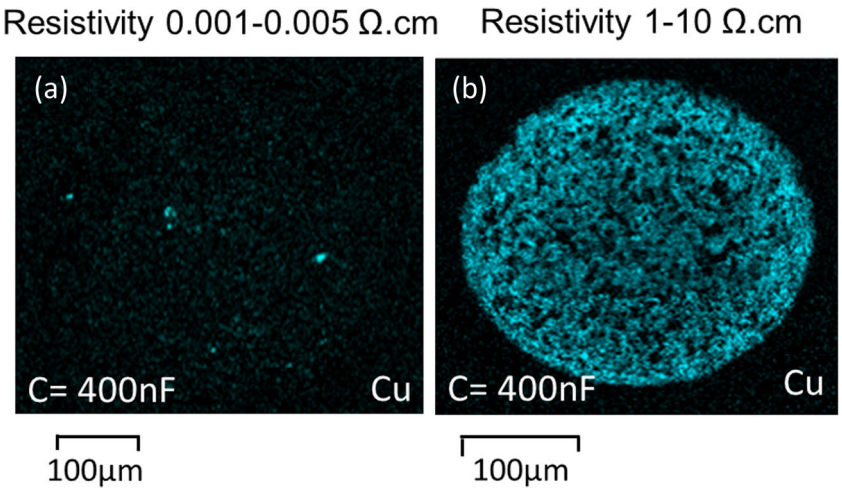

Fig. 10 EDX map images when 400 nF were used on low-resistivity sample (**a**) Cu and high-resistivity sample (**b**) Cu deposited

sample showed higher surface roughness compared to high-resistivity sample. It is worth noting that the increase of DE value caused by high spark employed to machine the workpiece, which resulted in rough cutting modes [34].

Figure 9 displays the result of surface roughness for both low- and high-resistivity samples when high voltage of 120 V with 10 nF (120 µJ) and high capacitance of 400 nF with 100 V (2000 µJ) were employed. The roughness of low-resistivity sample was 1.3416 µm and high resistivity sample was 0.731 µm at 120 µJ of DE. For the highest capacitance of 2000 µJ, the roughness for low resistivity sample was 2.5868 µm and the high resistivity sample was 1.2787 µm. These measurements show that the surface roughness is 2× higher for low-resistivity samples. This is due to the flow of current during the occurrence of discharge which is higher for low-resistivity sample. A relatively larger workpiece material melted when high DE is used due to the larger spark being generated and crater evidences were evident on the surface.

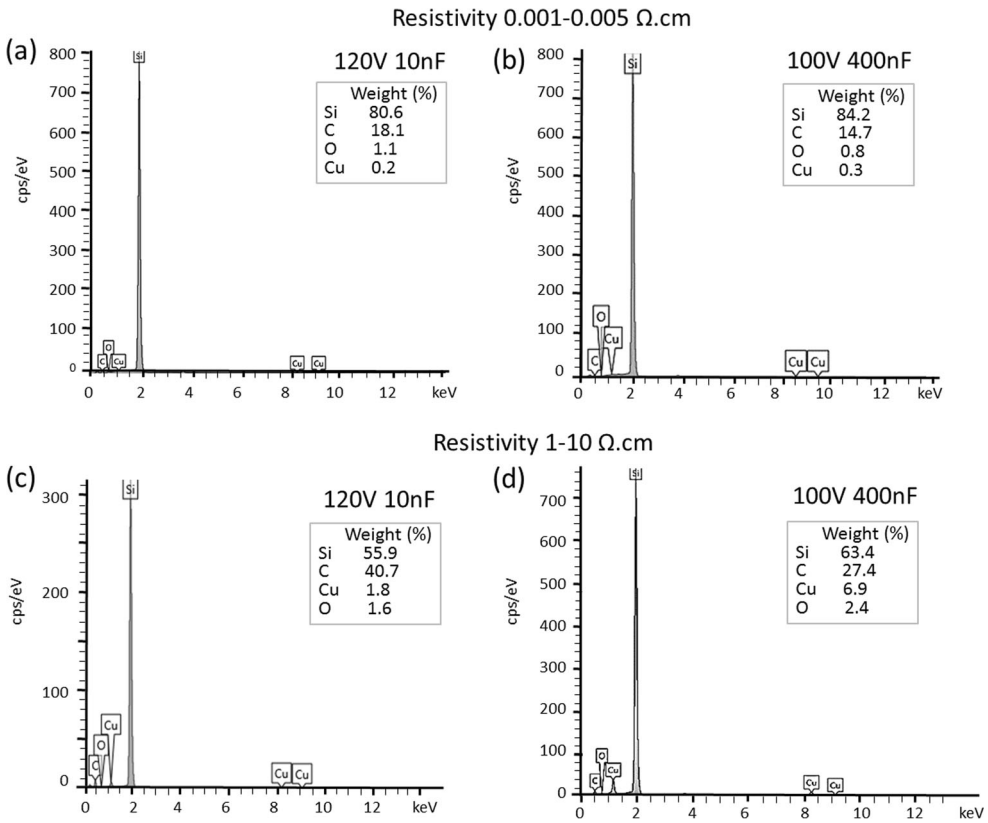

Fig. 11 EDX spectrum of the die-sinking µEDM: low-resistivity sample **a** 120 V, **b** 400 nF; high-resistivity sample **c** 120 V, **d** 400 nF

Similar to low-resistivity sample, the value of roughness for high-resistivity sample also showed an increase in the surface roughness when higher DE is used.

3.5 Materials deposition

Energy-dispersive X-ray spectroscopy (EDX) attached with FESEM was used to characterize the deposited elements in order to study the amount of material deposited into the drilled cavity. Major element in the electrode, namely, Cu, is observed in the machined cavity as shown in Fig. 10. The presence of Cu elements would be unpleasant in semiconductor material machining because they can influence the use of the substrate due to its diffusion. When identical DE is used (2000 μJ), the EDX maps of Cu elements were observed in the spark region of workpiece in Fig. 10a for low-resistivity sample and Fig. 10b for high-resistivity sample. Higher Cu deposition is observed on high-resistivity sample, as it requires longer machining time for cavity formation. When DE is set at low, the deposition of Cu detached from brass electrode is also expected to be high due to long machining time that gave more chance for the Cu to be deposited and melted on the workpiece surface.

The EDX analyses demonstrated in Fig. 11 showed the level of the main elements present in the machined cavities, which are based on the highest voltage and the highest capacitance parameters for both high- and low-resistivity samples. At 120 V with 10 nF (see Fig. 11a) and 100 V with 400 nF (see Fig. 11b), approximately eight times larger weight percentage of Cu was detected for high-resistivity samples. High-resistivity sample showed a relatively higher percentage of C and O compared to low-resistivity sample for both DEs. This indicated that longer machining time is needed for high-resistivity samples, which causes more Cu material to react and the presence of C debris around the machined cavity. Hence, more carbonized and oxidized layer remained in the cavity.

4 Conclusions

The present study investigates the two n-type Si wafers with 0.001–0.005 Ω cm and 1–10 Ω cm that were machined by means of the die-sinking μEDM technique with 300 μm diameter of brass electrode. Cavities with 100 μm depth were machined using a range of voltages (i.e., 80 to 120 V) at constant capacitance of 10 nF and a range of capacitances (0.1 to 400 nF) at constant voltage, 100 V to produce different DE from 0.5 to 2000 μJ, respectively. The effects of Si resistivity and DE on the μEDM machining performances were analyzed. The results obtained showed that the MRR for low-resistivity sample is higher than high-resistivity sample by factor of ~ 6 at low DE. In addition, shorter machining time that was required to machine the cavities on low-resistivity samples reduces the contamination of Cu, C, and O. Although the high resistivity, which resulted in low MRR required longer machining time and produced high level of contamination, the surface quality of high-resistivity sample is ~ 2× better than low-resistivity sample. For future work, further investigations on the tool electrode and it wear during machining, as well as simulation to evaluate the machining sensitivity are deemed necessary.

Acknowledgements This study is funded by Universiti Teknologi Malaysia under Matching Grant Scheme 00M83 and Research University Grant (GUP 14H31). Noor Dzulaikha Daud acknowledges the financial support from the Ministry of Education Malaysia under MyBrain15 scheme.

Compliance with ethical standards

Conflict of interest The authors declare that they have no conflict of interest.

References

1. Punturat J, Tangwarodomnukun V, Dumkum C (2014) Surface characteristics and damage of monocrystalline silicon induced by wire-EDM. Appl Surf Sci 320:83–92
2. Mingbo Q, Zhidong L, Zongjun T, Wei W, Yinhui H (2013) Study of unidirectional conductivity on the electrical discharge machining of semiconductor crystals. Precis Eng 37(4):902–907
3. Fang FZ, Venkatesh VC (1998) Diamond cutting of silicon with nanometric finish. CIRP Ann - Manuf Technol 47(1):45–49. https://doi.org/10.1016/S0007-8506(07)62782-6
4. Chan M, Fonda P, Reyes C, Xie J, Najar H, Lin L, Yamazaki K, Horsley D Micromachining 3D hemispherical features in silicon via micro-EDM. In: Micro Electro Mechanical Systems (MEMS), 2012 I.E. 25th International Conference on, 2012. IEEE, pp 289–292
5. Weinhold S, Gruner A, Ebert R, Schille J, Exner H Study of fast laser induced cutting of silicon materials. In: SPIE LASE, 2014. International Society for Optics and Photonics, pp 89671J-89671J-89677
6. Yu Z, Hu X, Rajurkar KP (2006) Influence of debris accumulation on material removal and surface roughness in micro ultrasonic machining of silicon. CIRP Ann - Manuf Technol 55(1):201–204. https://doi.org/10.1016/S0007-8506(07)60398-9
7. Xiao G, To S, Jelenković E (2015) Effects of non-amorphizing hydrogen ion implantation on anisotropy in micro cutting of silicon. J Mater Process Technol 225:439–450
8. Tang Y, Fuh J, Loh H, Wong Y, Lim Y (2008) Laser dicing of silicon wafer. Surf Rev Lett 15(01n02):153–159
9. Belyaev A, Polupan O, Dallas W, Ostapenko S, Hess D, Wohlgemuth J (2006) Crack detection and analyses using resonance ultrasonic vibrations in full-size crystalline silicon wafers. Appl Phys Lett 88(11):111907
10. Hung N, Fu Y, Ali MY (2002) Focused ion beam machining of silicon. J Mater Process Technol 127(2):256–260
11. Reynaerts D, Meeusen W, Van Brussel H (1998) Machining of three-dimensional microstructures in silicon by electro-discharge machining. Sens Actuators, A 67(1):159–165

12. Ali MSM, Bycraft B, Schlosser C, Assadsangabi B, Takahata K (2011) Out-of-plane spiral-coil inductor self-assembled by locally controlled bimorph actuation. Micro Nano Lett 6(12):1016–1018
13. Rahul S, Datta S, Biswal BB, Mahapatra SS (2017) Electrical discharge machining of Inconel 825 using cryogenically treated copper electrode: emphasis on surface integrity and metallurgical characteristics. J Manuf Process 26:188–202. https://doi.org/10.1016/j.jmapro.2017.02.020
14. Suresh Kumar S, Uthayakumar M, Thirumalai Kumaran S, Parameswaran P, Mohandas E, Kempulraj G, Ramesh Babu BS, Natarajan SA (2015) Parametric optimization of wire electrical discharge machining on aluminium based composites through grey relational analysis. J Manuf Process 20(Part 1):33–39. https://doi.org/10.1016/j.jmapro.2015.09.011
15. AbuZaiter A, Hikmat OF, Nafea M, Ali MSM (2016) Design and fabrication of a novel XYθz monolithic micro-positioning stage driven by NiTi shape-memory-alloy actuators. Smart Mater Struct 25(10):105004
16. AbuZaiter A, Nafea M, Faudzi AAM, Kazi S, Ali MSM (2016) Thermomechanical behavior of bulk NiTi shape-memory-alloy microactuators based on bimorph actuation. Microsyst Technol 22(8):2125–2131
17. Ali MSM, AbuZaiter A, Schlosser C, Bycraft B, Takahata K (2014) Wireless displacement sensing of micromachined spiral-coil actuator using resonant frequency tracking. Sensors 14(7):12399–12409
18. Khalid W, Ali MSM, Dahmardeh M, Choi Y, Yaghoobi P, Nojeh A, Takahata K (2010) High-aspect-ratio, free-form patterning of carbon nanotube forests using micro-electro-discharge machining. Diam Relat Mater 19(11):1405–1410
19. Dahmardeh M, Ali MSM, Saleh T, Hian TM, Moghaddam MV, Nojeh A, Takahata K (2013) High-power MEMS switch enabled by carbon-nanotube contact and shape-memory-alloy actuator. Phys Status Solidi (a) 210(4):631–638
20. Anwar MM, Saleh T, Madden JD, Takahata K (2014) Micropatterning polypyrrole conducting polymer by pulsed electrical discharge. Macromol Mater Eng 299(2):198–207
21. Heeren P, Reynaerts D, Van Brussel H Three-dimensional silicon micromechanical parts manufactured by electro-discharge machining. In: Advanced Robotics, 1997. ICAR'97. Proceedings., 8th International Conference on, 1997. IEEE, pp 247–252
22. Fonda P, Chan M, Heidari A, Nakamoto K, Sano S, Horsley D, Yamazaki K (2013) The application of diamond-based electrodes for efficient EDMing of silicon wafers for freeform MEMS device fabrication. Procedia CIRP 6:280–285
23. Reynaerts D, Van Brussel H (1997) Microstructuring of silicon by electro-discharge machining (EDM)—part I: theory. Sensors Actuators A 60(1):212–218
24. Saleh T, Rasheed AN, Muthalif AG (2015) Experimental study on improving μ-WEDM and μ-EDM of doped silicon by temporary metallic coating. Int J Adv Manuf Technol 78(9–12):1651–1663
25. Kunieda M, Ojima S (2000) Improvement of EDM efficiency of silicon single crystal through ohmic contact. Precis Eng 24(3):185–190
26. Unoa Y, Okada A, Okamoto Y, Yamazaki K, Risbud SH, Yamada Y (1999) High efficiency fine boring of monocrystalline silicon ingot by electrical discharge machining. Precis Eng 23(2):126–133. https://doi.org/10.1016/S0141-6359(98)00029-4
27. Yu P-H, Lin Y-X, Lee H-K, Mai C-C, Yan B-H (2011) Improvement of wire electrical discharge machining efficiency in machining polycrystalline silicon with auxiliary-pulse voltage supply. Int J Adv Manuf Technol 57(9–12):991–1001
28. Zhidong L, Haoran C, Huijun P, Mingbo Q, Zongjun T (2015) Automatic control of WEDM servo for silicon processing using current pulse probability detection. Int J Adv Manuf Technol 76(1–4):367–374
29. Yeh C-C, Wu K-L, Lee J-W, Yan B-H (2013) Study on surface characteristics using phosphorous dielectric on wire electrical discharge machining of polycrystalline silicon. Int J Adv Manuf Technol 69(1–4):71–80
30. Murray J, Fay M, Kunieda M, Clare A (2013) TEM study on the electrical discharge machined surface of single-crystal silicon. J Mater Process Technol 213(5):801–809
31. Song X, Reynaerts D, Meeusen W, Van Brussel H (2001) A study on the elimination of micro-cracks in a sparked silicon surface. Sensors Actuators A 92(1):286–291
32. Rajurkar K, Sundaram M, Malshe A (2013) Review of electrochemical and electrodischarge machining. Procedia CIRP 6:13–26
33. Gostimirovic M, Kovac P, Sekulic M, Skoric B (2012) Influence of discharge energy on machining characteristics in EDM. J Mech Sci Technol 26(1):173–179
34. Qian J, Steegen S, Vander Poorten E, Reynaerts D, Van Brussel H (2002) EDM texturing of multicrystalline silicon wafer and EFG ribbon for solar cell application. Int J Mach Tools Manuf 42(15):1657–1664. https://doi.org/10.1016/S0890-6955(02)00116-5